Check for updates

Advances in Materials Technology for Fossil Power Plants
Proceedings from the Seventh International Conference
October 22–25, 2013, Waikoloa, Hawaii, USA
https://doi.org/10.31399/asm.cp.am-epri-2013p1441

Copyright © 2014 Electric Power Research Institute, Inc.
Distributed by ASM International®. All rights reserved.
D. Gandy, J. Shingledecker, editors

A COMPUTATIONAL DESIGN STUDY OF NOVEL CREEP RESISTANT STEELS FOR FOSSIL FUEL POWER

Qi Lu, Wei Xu, Sybrand van der Zwaag
Novel Aerospace Materials group, Faculty of Aerospace Engineering, Delft University of Technology, 2629 HS, Delft, The Netherlands

ABSTRACT

This work concerns a study into the design of creep resistant precipitation hardened austenitic steels for fossil fuel power plants using an integrated thermodynamics based model in combination with a genetic algorithm optimization routine. The key optimization parameter is the secondary stage creep strain at the intended service temperature and time, taking into account the coarsening rate of MX carbonitrides and its effect on the threshold stress for secondary creep. The creep stress to reach a maximal allowed creep strain (taken as 1%) at a given combination of service temperature and time is formulated and maximized. The model was found to predict the behavior of commercial austenitic creep resistant steels rather accurately. Using the alloy optimization scheme three new steel compositions are presented yielding optimal creep strength for various intended service times up to 10^5 hours. According to the evaluation parameter employed, the newly defined compositions will outperform existing precipitate strengthened austenitic creep resistant steels.

1. INTRODUCTION

Creep resistant steels are widely used in fossil fuel power plants owing to their great properties at demanding conditions: elevated temperatures, high loads and long service times. During such conditions, the creep strain evolves and shows three stages: primary, secondary/steady and tertiary creep. Among these three stages, the secondary/steady stage is the most important one as it accounts for the largest part of creep life [1]. During secondary stage, the creep rate is constant and inversely proportional to the creep life according to the Monkman-Grant relationship [2], Moreover, in industry, the stress that produces a creep rate of 10^{-7}/ hour (or 1% strain for 10^5 hours) is taken as the maximum allowable stress.

Design of new creep resistant alloys by a traditional trial and error method is time consuming and expensive. Computational methods have been considered as an alternative way to design novel alloy in recent years. Computational thermodynamics [3-5], artificial neural networks (ANN) [6, 7] and ab initio calculations [8-10], have been developed to predict the optimal alloy composition for specified use conditions, and to guide and accelerate costly experimental alloy development programs. More recently, a thermodynamics based model in combination with genetic algorithm (GA) was developed and successfully applied to the design of novel Ultra High Strength (UHS) stainless steel grades for room temperature application [11-14]. This alloy design approach was further extended to the design of heat resistant precipitates strengthened steels [15], and focused on the high temperature strength evolution by taking into account the development of precipitates.

Downloaded from http://dl.asminternational.org/am-epri/proceedings-pdf/AM-EPRI2013/84666/1441/680536/epri2013p1441.pdf
by guest

However, in the latter approach, the creep strain during use itself, which essentially determines the creep failure, was not considered. The creep strain can be estimated by using constitutive equations which correlate the strain (rate) to the stress and the temperature. Some constitutive models have been developed based on experimental observations of strain-stress behavior [16]. Other models attempt to link creep behavior with microstructural parameters, such as inter-particle spacing [17, 18], leading to microstructure associated constitutive equations. These constitutive equations can be used either as an assessment of creep rupture life at a given stress, or for the prediction of the creep strength for an intended life time.

In the present work, the genetic alloy design approach of high temperature steels is further developed by introducing a new (secondary creep) strain based optimization criterion and taking the coarsening of the TiX carbonitrides and its effect on the creep threshold stress as the main strength determining microstructural parameter. The model is validated against experimental data for various commercial creep resistant steel grades. Using the alloy optimization scheme, three new steel compositions are presented yielding optimal creep strength at 1% allowed strain for various intended service times (10, 10^3, 10^5 h).

Remember that you should not re-state material that is readily available in the archival literature. Simply summarize it, and then add a reference or two.

2. MODEL DESCRIPTION

2.1 Design methodology

In line with the 'chains model' proposed by Olson [19], the design methodology presented here follows the direction from performance to properties, microstructures and eventually to the composition & processing conditions. The method relies on two key conversions, the 'translator' for the correlation from mechanical properties to desirable microstructures, and the 'creator' to link desirable microstructures to alloy composition/heat treatments employing established metallurgical principles [20]. In the present work, the translator needs to translate the required properties for creep resistant steels, such as high strength, good stability and decent oxidation or corrosion resistance, into desirable microstructures using known microstructure-property relationships. The tailored microstructure is chosen to be an austenitic matrix with MX carbonitride precipitates. Compositional and microstructural details of such steels are reported in our previous study [15]. Then, the creator should link the tailored microstructural features to a specific composition and related heat treatment parameters via employing various go/no-go criteria, which involve thermodynamic and kinetics calculations. All qualified solutions are then ranked according to a properly chosen optimization factor,. Considering the large space of the pre-defined compositional domain, a Genetic Algorithm is employed to make sure the space is searched effectively and efficiently.

In the previous design study of heat resistant precipitation strengthened steels [15], the maximum precipitation strengthening contribution of MX carbonitrides at the intended time of use was considered as the optimization criterion. While the method yielded interesting suggestions for optimal compositions, it can be argued that precipitate coarsening rate is an indirect optimization parameter. Hence, it may be more appropriate to take the creep strain development itself as the direct optimization parameter.

Downloaded from http://dl.asminternational.org/am-epri/proceedings-pdf/AM-EPRI2013/84666/1441/680536/epri2013p1441.pdf
by guest

Creep behavior can be divided into diffusional and dislocation creep depending on the service temperature and applied stresses. According to Harnold and Ashby's deformation map for 316 austenitic stainless steel [21], advanced austenitic creep resistant steels will undergo dislocation creep at the intended service condition i.e. a service temperature of 650 °C and an applied stress higher than 60 MPa. For this type of creep mechanism various failure models have been proposed. Some researchers focused on the rupture due to void, grain boundary wedge accumulation and tried to correlate the damage with the rupture strength and hence to design austenitic and ferritic creep resistant steels [22-24] accordingly. Alternatively, others focused on the strain damage [25] and investigated effects of stress and temperature on strain rate and accumulated strain, especially in the secondary/steady stage [1, 26]. Our work will follow the latter approach, and the choice of equations to describe strain-stress and other new the model features are presented in the following.

Based on numerous experimental results involving various types of pure metals and precipitate free alloys [1], a power law equation of dependence of strain rate upon applied stress has been proposed and is now commonly accepted for estimating the strain rate during the steady stage [1]:

$$\dot{\varepsilon}_{ss} = C\exp(-Q/RT)(\frac{\sigma}{G})^n \tag{1}$$

where ε_{ss} is creep rate of steady stage. C is a constant, Q is activation energy, R is gas constant, T is temperature, σ is applied stress, G is shear modulus, component n is a constant normally ranging from 4 to 6. However, in the case of precipitate strengthened alloys the creep rate is not properly described by equation 1 and a threshold stress σ_{th} has been introduced [27]. If the applied stress is lower than the threshold stress, the strain rate is negligible and can be ignored. When it reaches the threshold stress, the strain rate will increase significantly with further increase of the applied stress. Thus, for precipitate strengthened alloys, equation (1) is reformulated as,

$$\dot{\varepsilon}_{ss} = C\exp(-Q/RT)(\frac{\sigma-\sigma_{th}}{G})^n \tag{2}$$

In equation (2), the component n will again be in the range 4 to 6. In our further analysis a fixed value for n, n=5, is imposed. According to Ref. [1], the threshold stress can be expressed as,

$$\sigma_{th} = \alpha Gb/L \tag{3}$$

where, α is a constant, G the shear modulus and L the average inter-particle spacing. For general dislocation climb, α varies from 0.004 to 0.02, for local climb, α=0.19 [1]. According to the detachment model [28] α is not a constant but changes with the mechanism of dislocations passing the particle. However, as a first order approximation α can be taken as being constant and equal for alloys with a common dislocation-precipitate interaction mode. In this work, the dimensionless factor α is taken as a constant, α = 0.02. The validity of this assumption will be tested and demonstrated in the results section using a range of experimental alloys.

In precipitation strengthened creep resistant steels, the precipitates evolve in time and hence the inter-particle spacing increases and threshold stress decreases with service time due to the coarsening of precipitates [29, 30]. According to LSW law [31, 32] the evolution of particle size with time can be expressed as

Downloaded from http://dl.asminternational.org/am-epri/proceedings-pdf/AM-EPRI2013/84666/1441/680536/epri2013p1441.pdf
by guest

$$L = r / \sqrt{f_p} = \sqrt[3]{r_0^3 + Kt} / \sqrt{f_p} \quad (4)$$

in which f_p, K and r_0 are the equilibrium volume fraction, coarsening rate and critical nuclei radius of the strengthening precipitates (TiX carbonitride in the current study) at the service temperature, respectively and t is time. r_0 can be expressed as

$$r_0 = 2\gamma / \Delta G_v \quad (5)$$

where γ is matrix-precipitate interfacial energy, ΔG_v is thermodynamic driving force for the precipitation. The coarsening rate K of a multi-component precipitate can be estimated by the equation proposed by Ågren[33]:

$$K = 8\gamma {V_m}^p / \sum_{i=1}^{n} \frac{9(x_i^p - x_i^{mp})^2}{x_i^{mp} D_i / RT} \quad (6)$$

where γ is matrix-precipitate interfacial energy, V_{mp} is the molar volume of precipitate. and t is the exposure time at the high temperature. x is the equilibrium interface mole fraction of the MX carbonitride forming elements on both the matrix (m) and the precipitate (p) side of the interface. R is gas constant, T is the service temperature and D is the corresponding diffusion coefficient. In the present work, the interfacial energy is arbitrarily set at a fixed value of 1 J/m^2 irrespective of the precipitate size. This is a slight simplification but allows illustrating the effect of precipitate coarsening more easily. All thermodynamic information including f_p, ΔG_v, x_i^p, x_i^{mp}, D_i and V_{mp} are calculated by employing Thermo-Calc coupled with TCFE6 and Mob2 databases.

The creep strain during the secondary stage therefore can be calculated by integrating equation (2) over time, while taking into account that the threshold stress is time dependent, as shown in formula (7):

$$\varepsilon = \int \dot{\varepsilon}_{ss} dt = \int C_1 \exp(-Q/RT)\left(\frac{\sigma - \sigma_{th}}{G}\right)^5 dt = C_2 \int \left(\sigma - \frac{\alpha G b \sqrt{f}}{\sqrt[3]{(r_0^3 + Kt)}}\right)^5 dt \quad (7)$$

Where C_2 is expressed as,

$$C_2 = \frac{C_1 \exp(-Q/RT)}{G^5} \quad (8)$$

C_2 is a constant for a certain temperature.

We are aware of the fact that the threshold stress not only depends on the initial size, coarsening rate and volume fraction of TiX carbonitride (equation (4)), but also changes with applied stress/creep rate [29]. In the current model, this second order effect has not been taken into account as there is not enough experimental data for precipitation hardened austenitic steels of different compositions available to numerically include the effect in the optimization process in a proper manner.

From equation (7), it can be deduced that, for a certain creep strain ε, a higher volume fraction of precipitate f and/or a smaller initial size r_0 and/or a smaller coarsening rate K will result in a

Downloaded from http://dl.asminternational.org/am-epri/proceedings-pdf/AM-EPRI2013/84666/1441/680536/epri2013p1441.pdf
by guest

higher allowable stress σ (i.e. in a higher creep strength). Since equation (7) is only suitable for the secondary stage, the selected strain level should be located within secondary creep range. According to the literature, the maximum strain for the secondary stage is up to around 1% for MX carbonitride strengthened austenitic heat resistant steels. Once it enters the tertiary stage, creep rate increases dramatically and the sample fails rapidly. This is also in agreement with the practical rule that the stress leading to 1% strain for the intended service time should be used as the allowable stress in its design. As a result, in this work we chose the maximal stress for a given combination of time and temperature to reach 1% strain as the optimization parameter. At given temperature, time and strain, for a given steel composition, the applied stress can be determined by solving equation (7) and be further optimized by the genetic algorithm. The actual algorithm and the positions of various go/no-go criteria (to be explained in the next section) are indicated in Fig. 1.

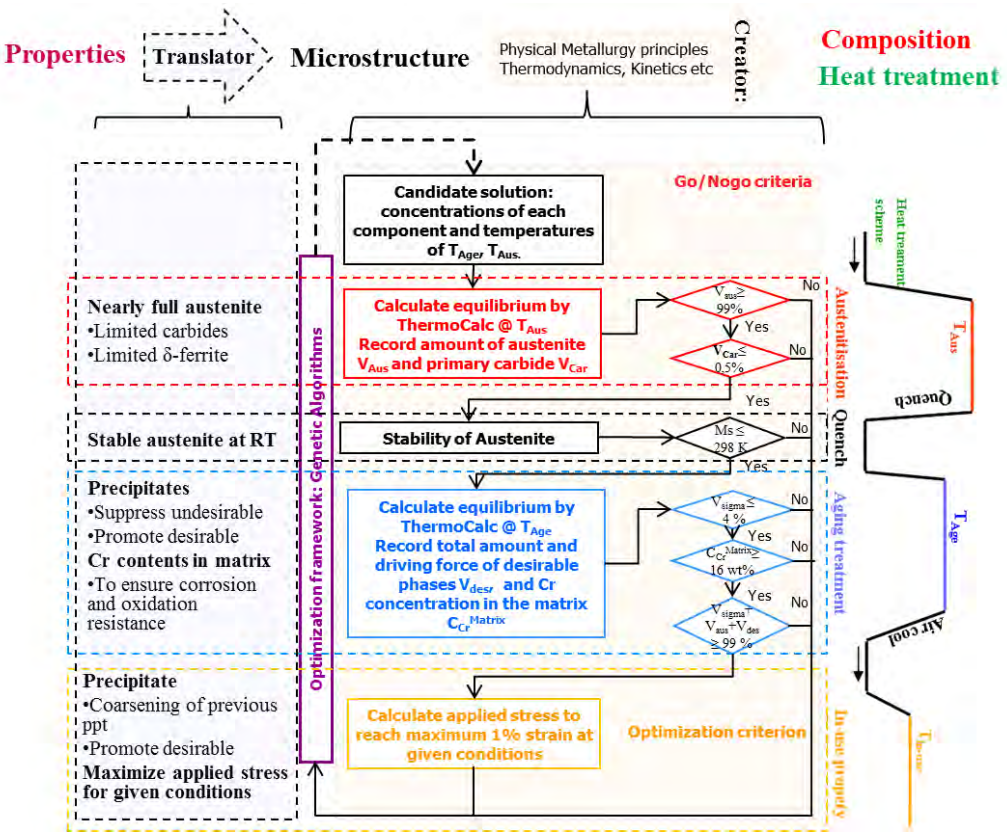

Figure 1 Alloy design strategy and criteria evaluation of high strength austenitic heat resistant steels.

2.3 Defining the go/no-go criteria

For MX carbonitride precipitation strengthened steels, the size, density and spatial distribution of precipitates together influence the threshold stress and affect the creep strength. In order to achieve the most desirable combination of threshold strength and stability of TiX carbonitrides, a proper heat treatment scheme is necessary. A typical heat treatment of precipitation strengthened

Downloaded from http://dl.asminternational.org/am-epri/proceedings-pdf/AM-EPRI2013/84666/1441/680536/epri2013p1441.pdf
by guest

steel includes an austenisation/solution treatment for dissolving undesirable primary carbonitrides and achieving compositional homogeneity, followed by a proper ageing treatment to form desirable precipitates. For creep resistant steels strengthened by TiX precipitates, a pre-ageing process to form the strengthening precipitates is usually not imposed as the desirable secondary strengthening MX carbonitrides will form during creep at elevated temperature anyway. Therefore, the ageing temperature and service temperature are considered to be the same. Various go/no-go criteria reflecting different metallurgical/microstructural considerations, shown in Fig. 1, are employed and are justified below

Following the order of heat treatment scheme, in the calculations in the optimization procedure each candidate alloy will receive an austenisation treatment first, hence a first thermodynamic calculation is performed at the austenisation temperature T_{Aus}. Two go/no-go criteria are imposed for this step, being (1) the equilibrium austenite volume at that temperature fraction should be larger than 99% and (2) the maximum level of primary carbides is limited to 0.5% in volume. After austenisation, the alloy will be cooled down to room temperature, and the austenite should remain intact and be stable. Therefore, a third go/no-go criterion being: Martensite start (T_{Ms}) temperature ≤25 °C , is imposed. The Ms temperature is calculated according to formula proposed by Ishida [34]:

$$T_{Ms}(°C)=545 - 33000W_C + 200W_{Al} + 700W_{Co} - 1400W_{Cr} - 1300W_{Cu} - 2300W_{Mn} - 500W_{Mo} - 400W_{Nb} - 1300W_{Ni} - 700W_{Si} + 300W_{Ti} + 400W_V \quad (9)$$

where W_i is the mass fraction for element "i".

After cooling to room temperature, the alloy will be used at its service/ageing temperature. Hence a second set of thermodynamic calculations at the service temperature are performed. Three additional go/no-go criteria are enforced: (4) the maximum allowed volume fraction for all undesirable phases (sigma phase excluded) together is set at 1 vol.%, (5) a minimum of 16 mass% Cr in the matrix upon completion of the precipitation reactions is imposed to ascertain adequate corrosion and oxidation resistance, and (6), the maximal allowed sigma phase (not functioning as strengthening precipitates) is set at 4 vol.%.

The candidate solutions which fulfil all go/no-go criteria (1)–(6), are then further evaluated by the optimization criteria according to equation (7), so as to maximize the allowed maximal stress leading to 1% strain at the predefined service temperature in the predefined (minimal) service time.

2.4 Searching condition and optimization framework

The composition ranges, heat treatment parameters and service times applied in the alloy design calculations are summarized in Table 1. In this analysis the ageing/service temperature is set at 650 °C. For this temperature, three service times (10 h, 10^3 h, 10^5 hours) are considered.

Table 1 Search ranges of composition (in mass%) and austenitisation temperature T_{aus} (in ^oC), service temperature T_{ser} = Ageing temperature T_{Age} (in ^oC). Mn level and Si level are fixed at 1.00 and 0.5 mass% respectively.

	C	*Cr*	*Ni*	*Ti*	*Mo*	*Cu*	*N*	T_{aus}	*Fe*	$T_{age}=T_{ser}$	Service/coarsening time and strain
MIN	0,01	15.00	8.00	0,01	0,10	0,01	0,01	1000	Bal.	650	10h-1%, 10^3h-1%, 10^5 h -1%
MAX	0,15	25.00	25.00	1.00	3.00	5.00	0,15	1250			

Downloaded from http://dl.asminternational.org/am-epri/proceedings-pdf/AM-EPRI2013/84666/1441/680536/epri2013p1441.pdf
by guest

A Genetic Algorithm is applied as the optimization scheme, taking into account 8 variables (7 alloying elements and the austenitization temperature) while setting 32 equally spaced levels between minimal and maximal values for each variable, yielding in total 328 candidate solutions. The composition and heat treatment parameters are coded in a 40 (5x8) bits binary string. More details of the genetic algorithm used can be found in a previous publication [11]. The calculation time to find the optimal solution in each design round is usually around 2 weeks using a high-end PC.

3. VALIDATION AND APPLICATION

3.1 Validation against reported experimental data

First of all, we like to reproduce experimental creep data at a fixed temperature of 650 °C for a well-known creep steel 321H [35] and to justify the use of the time to reach 1% strain as the appropriate creep resistance indicator. The experimental data are shown in Fig. 2. Figure 2a clearly shows that the time to reach 1 % strain (indicated by dashed line) forms a substantial and more or less constant fraction of the total creep life time, irrespective of the imposed stress level, in accordance with the Monkman-Grant relationship [2]. Taking the composition of 321H and calculating the initial precipitate size (equation) and the coarsening rate (equation 6) and inserting the appropriate values into the final creep strain equation (equation 7) the time to reach 1% creep strain was calculated. The calculated time to reach 1% strain (using a value of $C_2 = 2.23*10^{47}$ as the calibration factor) is compared to the experimental value in Fig. 2b and a very good agreement over the entire stress range of 53-216 MPa is obtained.

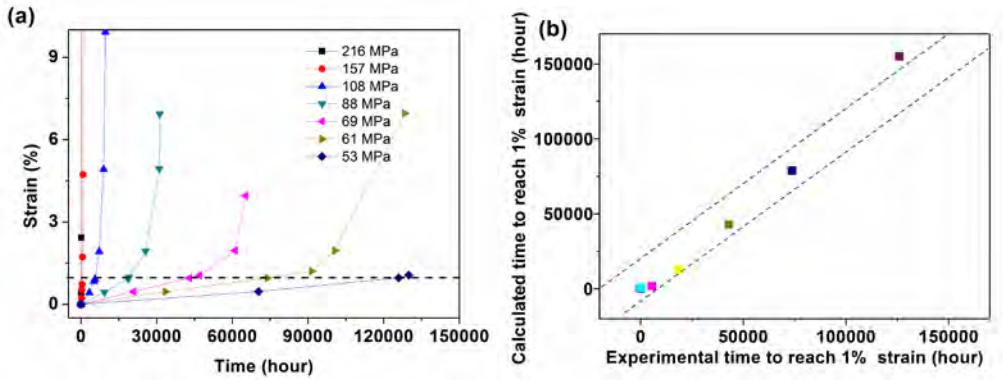

Figure 2 a) Actual creep strain evolution with time at various stress levels for 321H after [35]. b) model predictions for the time to reach 1% strain versus the experimentally determined time to reach 1% strain at various stress levels

Secondly, in Fig. 3a the relationship between the experimental life time (creep rupture time) at fixed temperature of 650 °C and the applied stress is plotted for 5 commercial precipitation hardened austenitic creep steels. The compositions of the 5 steel grades are listed in table 2.

Downloaded from http://dl.asminternational.org/am-epri/proceedings-pdf/AM-EPRI2013/84666/1441/680536/epri2013p1441.pdf
by guest

Table 2 : Chemical compositions of the 5 commercial steels presented in Fig. 3 (in mass%)

	C	*Cr*	*Ni*	*Ti*	*Mo*	*Nb*	*N*	*Mn*	*Si*
16-13Nb	0,07	16	11			0,7		1	0,5
321H	0,07	18,5	11	0,3				1	0,5
347H	0,08	18,5	11			0,64		1	0,4
NF709	0,04	22,29	24,87	0,02	1,42	0,23	0,18	0,97	0,4
TEMPALOY-1	0,12	18	10	0,08		0,1		1	0,6

It is clear that the compositions of all 5 steel grades are well within the final compositional space to be explored in this optimization (see table 1) except for the N level for NF 709, which is only a little greater than the maximum value set. For all alloys except TEMPALOY A-1, there is only one type of MX carbonitride (as is assumed in the present design study). For TEMPALOY A-1, there are two types of MX (TiX and NbX) carbonitrides, and the coarsening behavior of each of them are completely different. Therefore, the time-stress curve of TEMPALOY A-1 crosses that of the other grades.

In Fig. 3b, the calculated stress for these 5 steel grades to reach 1% strain after 10^4 hours' service at 650 °C is compared to the experimental rupture stress values. There is a very good correspondence. As is to be expected the rupture stress is slightly greater than the predicted stress for 1% strain for the same service time, since the rupture strain is normally greater than 1%. For other service times the prediction of the relative ranking of the 5 steel grades is equally good, albeit that the relative behavior of TEMPALOY A-1 sometime deviates a bit due to the role of its NbX carbonitrides, which are not taken into account in the model. It should be noted that the same C_2 value (calibrated by using data from 321H) was used for all 5 steel compositions, suggesting that in the optimization over the composition domain defined in table 1, the use of a constant calibration factor C2 is likely to be an acceptable simplification.

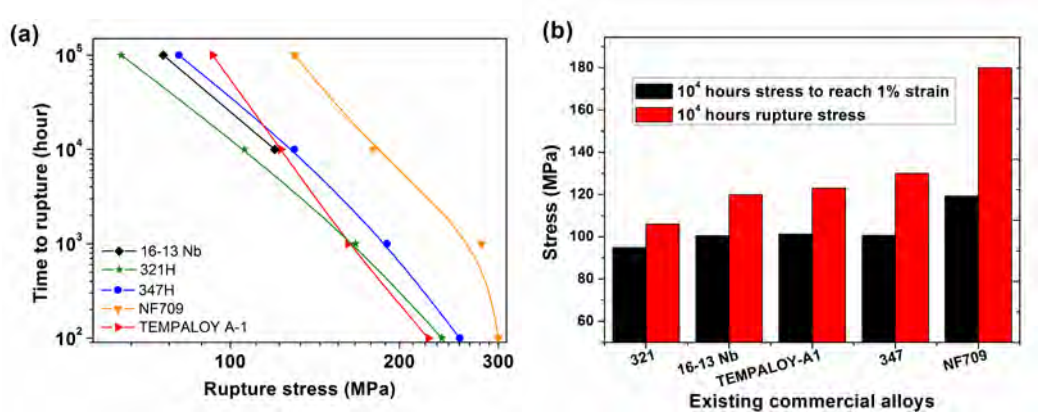

Figure 3 (a) Experimental rupture time dependence of (applied) stress for various existing commercial steel grades [35, 36]. (b) Comparison of experimental rupture stress and the calculated stress to reach 1% strain in 10^4 hours .

The very good agreement between predicted and experimental data for industrial grades demonstrated in Figs. 2 and 3 should give some credibility to the predictions to be made with the model for steel compositions not yet explored experimentally.

Downloaded from http://dl.asminternational.org/am-epri/proceedings-pdf/AM-EPRI2013/84666/1441/680536/epri2013p1441.pdf
by guest

3.2 Design results

To design alloys suitable for different service conditions, three values for the intended service time (i.e. the time to reach 1% strain) were selected according to practical service conditions, i.e. 10h - 10^3 h - and 10^5 h respectively. The three selected time scales correspond to short, intermediate and long term creep conditions respectively. The resulting optimized alloy compositions for the three creep conditions are named alloy 1, alloy 2 and alloy 3 respectively, and their compositions are listed in Table 3. For each of the alloying elements the three predicted optimal values are located well within search region except for the molybdenum concentration which is at the lower boundary value. The low Mo concentration value coming out of the optimisation is attributed to the tendency of Mo to promote the formation of the undesirable Sigma phase (go/no-go criterion No. 6).

Table 3 The composition (in mass%), austenitisation temperature T_{aus} (in ^{o}C), Service temperature T_{age} = Ageing temperature T_{ser} (in ^{o}C), service time (in hours) and strain of the designed alloys.

	C	*Cr*	*Ni*	*Ti*	*Mo*	*Cu*	*N*	*Mn*	*Si*	$T_{age}=T_{ser}$	T_{aus}	*Strain*	$t_{service(hr)}$
Alloy 1	0,015	16,29	24,45	0,23	0,10	1,05	0,06	1.00	0.50	650	1250	1%	10
Alloy 2	0,019	16,29	22,81	0,20	0,10	0,89	0,064	1.00	0.50	650	1161,3	1%	10^3
Alloy 3	0,051	17,58	17,87	0,17	0,10	0,10	0,055	1.00	0.50	650	1178,5	1%	10^5

In order to visualize the differences in time dependent behavior of the three alloys, the stresses leading to 1 % strain as a function of time are plotted in Fig. 4. The Figure clearly indicates that each steel grade outperforms the other two grades at its designed lifetime (indicated by arrows) which demonstrates the effectiveness of the GA optimization procedure as such. Alloy 1 designed for 10 h shows the fastest reduction in allowed stress as a function of the service time. Alloys 2 and 3 almost have more or less the same degradation behavior, and the maximal stresses for short time services are only slightly lower than that of alloy 1. Nevertheless, the maximum imposable stresses decrease much more slowly than that for alloy 1, and have a much higher value at a service time of 10^3 h and beyond. The predicted relative 'strength' of alloys 2 and 3 at the intended service times of 10^3 and 10^5 hours are in their intended mutual position, but the difference in absolute value is small.

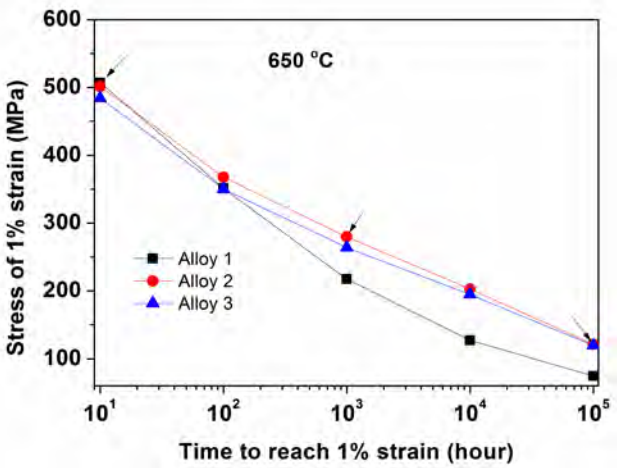

Figure 4 The calculated stress of 1% strain versus time to reach 1% strain for the three alloys designed to give optimal strength at 0, 10 and 10^5 hour at 650 $^{°C}$ respectively.

Downloaded from http://dl.asminternational.org/am-epri/proceedings-pdf/AM-EPRI2013/84666/1441/680536/epri2013p1441.pdf
by guest

3.3 The comparison of designed alloys and existing commercial steel grades

To show the predicted improvement in maximum allowed stress for the two new alloys (alloys 2 and 3), the maximum allowable stresses and the experimentally determined creep strength values at both 10^4 and 10^5 hours are plotted in Fig. 5. As shown in Fig. 5, the experimental allowable stresses for the 5 reference steels can be well predicted using equation (7) the fixed C2 value presented earlier. Given the excellent agreement between predictions and experimental data for the commercial steels, we conclude that the newly designed alloys 2 and 3, with intended service lifetimes of 10^3 and 10^5 hours are likely to have substantially higher creep strength values than the currently existing precipitation hardened austenitic steels.

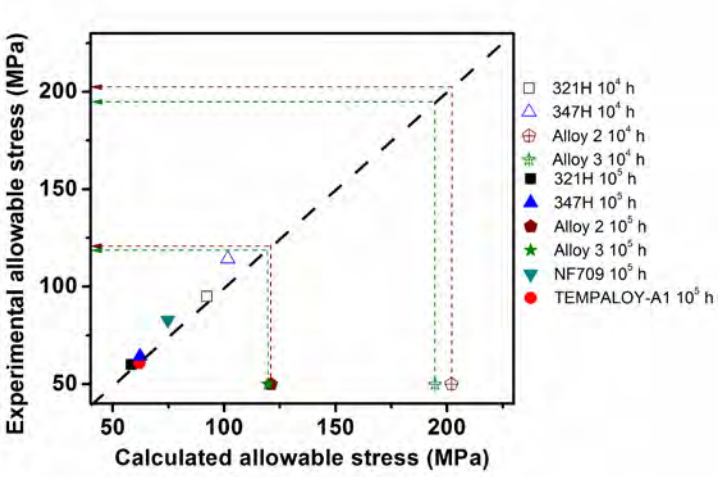

Figure 5 comparison of predicted and experimental maximal allowable stress values for experimental steel grades [35, 36] (at either 10^4 or 10^5 hours) as well as the calculated allowable stress and resulting predicted resulting allowable stress for alloys 2 and 3 (see legenda)

4. CONCLUSIONS

A strain based computational model for the design of creep resistant steels, which takes into account the coarsening of TiX carbonitride precipitates and its effect on threshold stress, was able to reproduce the properties of existing precipitation hardened austenitic creep resistant steels with very good accuracy. The wider exploration of the compositional domain involving 7 alloying elements and an adjustable austenisation temperature, led to the definition of new alloy compositions predicted to have substantially better properties at 650 °C (both for short, medium and long service times) than the existing commercial steel grades.

ACKNOWLEDGEMENT

This work was carried out with financial support from the Chinese Scholarship Council (CSC) as well as internal TU Delft funding.

Downloaded from http://dl.asminternational.org/am-epri/proceedings-pdf/AM-EPRI2013/84666/1441/680536/epri2013p1441.pdf
by guest

REFERENCES

[1] M.E. Kassner, M.-T. Pérez-Prado, Fundamentals of creep in metals and alloys, Elsevier (Amsterdam), 2004.
[2] F.C. Monkman, N.J. Grant, An empirical relationship between rupture life and minimum creep rate in creep-rupture tests, Proc. ASTM, 56 (1956) 593-620.
[3] J. Hald, L. Korcakova, H.K. Damelsen, K.V. Dahl, Thermodynamic and kinetic modelling: Creep resistant materials, Mater. Sci. Technol., 24 (2008) 149-158.
[4] Z.K. Teng, F. Zhang, M.K. Miller, C.T. Liu, S. Huang, Y.T. Chou, R.H. Tien, Y.A. Chang, P.K. Liaw, New NiAl-strengthened ferritic steels with balanced creep resistance and ductility designed by coupling thermodynamic calculations with focused experiments, Intermetallics, 29 (2012) 110-115.
[5] V. Knežević, J. Balun, G. Sauthoff, G. Inden, A. Schneider, Design of martensitic/ferritic heat-resistant steels for application at 650 °C with supporting thermodynamic modelling, Mater. Sci. Eng., A, 477 (2008) 334-343.
[6] V. Venkatesh, H.J. Rack, A neural network approach to elevated temperature creep-fatigue life prediction, Int. J. Fatigue, 21 (1999) 225-234.
[7] H.K.D.H. Bhadeshia, Design of ferritic creep-resistant steels, ISIJ Int., 41 (2001) 626-640.
[8] Z. Guo, W. Sha, Modelling the correlation between processing parameters and properties of maraging steels using artificial neural network, Computational Materials Science, 29 (2004) 12-28.
[9] W.A. Counts, M. Friák, D. Raabe, J. Neugebauer, Using ab initio calculations in designing bcc Mg-Li alloys for ultra-lightweight applications, Acta Mater., 57 (2009) 69-76.
[10] L. Vitos, P.A. Korzhavyi, B. Johansson, Stainless steel optimization from quantum mechanical calculations, Nat. Mater., 2 (2003) 25-28.
[11] W. Xu, P.E.J. Rivera-Díaz-del-Castillo, S. van der Zwaag, Designing nanoprecipitation strengthened UHS stainless steels combining genetic algorithms and thermodynamics, Comput. Mater. Sci., 44 (2008) 678-689.
[12] W. Xu, P.E.J. Rivera-Díaz-Del-Castillo, S. van der Zwaag, Genetic alloy design based on thermodynamics and kinetics, Philos. Mag., 88 (2008) 1825-1833.
[13] W. Xu, P.E.J. Rivera-Díaz-del-Castillo, W. Yan, K. Yang, D. San Martín, L.A.I. Kestens, S. van der Zwaag, A new ultrahigh-strength stainless steel strengthened by various coexisting nanoprecipitates, Acta Mater., 58 (2010) 4067-4075.
[14] W. Xu, P.E.J. Rivera-Díaz-del-Castillo, W. Wang, K. Yang, V. Bliznuk, L.A.I. Kestens, S. van der Zwaag, Genetic design and characterization of novel ultra-high-strength stainless steels strengthened by Ni3Ti intermetallic nanoprecipitates, Acta Mater., 58 (2010) 3582-3593.
[15] Q. Lu, W. Xu, S. van der Zwaag, Computational design of precipitation strengthened austenitic heat resistant steels, Philos. Mag., DOI:10.1080/14786435.2013.809493, (2013).
[16] G. Merckling, Long-term creep rupture strength assessment: Development of the European Collaborative Creep Committee post-assessment tests, Int. J. Press. Vessels Pip., 85 (2008) 2-13.
[17] B. Reichert, Y. Estrin, H. Schuster, Implementation of precipitation and ripening of second-phase particles in the constitutive modelling of creep, Scr. Mater., 38 (1998) 1463-1468.
[18] B.F. Dyson, Microstructure based creep constitutive model for precipitation strengthened alloys: Theory and application, Mater. Sci. Technol., 25 (2009) 213-220.
[19] G.B. Olson, Computational design of hierarchically structured materials, Science, 277 (1997) 1237-1242.
[20] W. Xu, Q. Lu, X. Xu, S. van der Zwaag, The structure of a general materials genome approach to the design of new steel grades for specific properties, Computer method in materials science, in press.

Downloaded from http://dl.asminternational.org/am-epri/proceedings-pdf/AM-EPRI2013/84666/1441/680536/epri2013p1441.pdf
by guest

[21] H.J. Frost, M.F. Ashby, Deformation-Mechanism Maps: The Plasticity and Creep of Metals and Ceramics, Pergamon press (Oxford), 1982.
[22] J. Lin, Y. Liu, T.A. Dean, A review on damage mechanisms, models and calibration methods under various deformation conditions, Int. J. Damage Mech, 14 (2005) 299-319.
[23] S.W. Nam, Assessment of damage and life prediction of austenitic stainless steel under high temperature creep-fatigue interaction condition, Mater. Sci. Eng., A, 322 (2002) 64-72.
[24] V. Sklenička, V. Šustek, I. Saxl, J. Čadek, An assessment of time and strain to creep fracture in a low alloy heat-resistant CrMoV steel based on a physical-metallurgical approach, Mater. Sci. Eng., 62 (1984) 1-9.
[25] Y. Estrin, Y. Bréchet, Damage nucleating at second-phase particles: A constitutive model, Scr. Mater., 35 (1996) 1057-1064.
[26] F. Garofalo, Fundamentals of creep and creep-rupture in metals, The Macmillan Company(New York), 1965.
[27] R.W. Lund, W.D. Nix, High temperature creep of Ni-20Cr-2ThO2 single crystals, Acta Metall., 24 (1976) 469-481.
[28] J. Rösler, E. Arzt, A new model-based creep equation for dispersion strengthened materials, Acta Metall. Mater., 38 (1990) 671-683.
[29] R.A. Stevens, P.E.J. Flewitt, The dependence of creep rate on microstructure in a γ′ strengthened superalloy, Acta Metall., 29 (1981) 867-882.
[30] K.R. Williams, B.J. Cane, Creep behaviour of 1/2Cr 1/2Mo 1/4V steel at engineering stresses, Mater. Sci. Eng., A, 38 (1979) 199-210.
[31] I.M. Lifshitz, V.V. Slyozov. The kinetics of precipitation from supersaturated solid solutions. J. Phys. Chem. Solids, 19 (1961) 35-50.
[32] C. Wagner, Theorie der Alterung von Niederschlägen durch umlösen, Zeitschrift für Elektrochemie, 65 (1961) 581-591.
[33] J. Ågren, M.T. Clavaguera-Mora, J. Golczewski, G. Inden, H. Kumar, C. Sigli, Applications of Computational Thermodynamics: Group 3: Application of computational thermodynamics to phase transformation nucleation and coarsening, Calphad-Computer Coupling of Phase Diagrams and Thermochemistry, 24 (2000) 41-54.
[34] K. Ishida, Calculation of the effect of alloying elements on the Ms temperature in steels, J. Alloys Compd., 220 (1995) 126-131.
[35] NIMS creep data sheet, National institute for materials science, http://smds.nims.go.jp/creep/index_en.html
[36] Specialty steels and heat-resistant alloys, Properties and selection: iron, steels and high performance alloys, ASM Handbook: ASM International, 2005.

Downloaded from http://dl.asminternational.org/am-epri/proceedings-pdf/AM-EPRI2013/84666/1441/680536/epri2013p1441.pdf
by guest